

INVESTIGATIONS INTO THE CRACKING BEHAVIOUR OF EPOXY-IMPREGNATED TEXTILE-REINFORCED CONCRETE

Philipp Preinstorfer^{*1,2}, Serdar Yanik³, Johannes Kirnbauer³, Agathe Robisson³

¹ Department of Engineering, University of Cambridge, Cambridge, United Kingdom

² Institute of Structural Engineering, TU Wien, Vienna, Austria

³ Institute of Material Technology, Building Physics, and Building Ecology, TU Wien, Vienna, Austria

*Corresponding author email: pp541@cam.ac.uk

Abstract

Textile-reinforced concrete is a novel composite material consisting of high-performance textile fabrics and high-strength concrete. Due to differences in the shape and the mechanical properties of the reinforcement, a direct transfer of existing knowledge on the bond behaviour of steel reinforcement is not possible. While it has been shown in the past that the geometric properties of the textile reinforcement are essential parameters that influence the bond properties, few investigations have been carried out on the cracking behaviour of textile-reinforced concrete itself. In this paper, the results of an extensive experimental campaign on the crack progression in textile-reinforced concrete elements under uniaxial tension is presented. In total 48 test specimens with different geometric properties and different surface characteristics were monitored during testing with advanced measuring techniques such as digital image correlation (DIC). This allows for an evaluation of the crack widths at different load stages. Additionally, laser scans on all tested fibre strands were conducted in order to get 3d-models of the different fabrics used. The geometry determined from these scans is linked to the results from the uniaxial tensile tests. The results clearly indicate the dependence of the cracking behaviour on the shape of the different textile types. Furthermore, if the crack width is a decisive criterion in the serviceability limit state, an additional sand coating guarantees smaller crack widths and distances.

Keywords: *textile reinforcement; CFRP-reinforcement, eco-efficiency, environmental impact; functional graded concrete*

1. INTRODUCTION

Textile reinforcement is a novel type of reinforcement consisting of bundles of continuous fibres that are processed into a fabric using highly-automized textile fabrication methods [1]. Textile-reinforced concrete (TRC) allows for the creation of lightweight and durable structures [2-5]. State of the art nowadays is to impregnate these fabrics to better activate the individual filaments and thus increase the performance of the material [6]. In new buildings, an economic driven trend for using epoxy-impregnated textiles with a high yarn count is noticeable [7-9], as epoxy impregnated textiles generally provide the best mechanical performance. This is accompanied by a significantly improved bond performance of the textile reinforcement in the concrete [10].

The cracking behaviour of composite structures is directly influenced by the bond performance of the reinforcement embedded in the cementitious matrix. If the reinforcement exhibits a repeating variation in cross-sectional dimensions, mechanical interlock with the surrounding concrete can be achieved [11, 12], while otherwise friction and adhesion are the main bond parameters. This is because the variation in cross-sectional dimensions, which is a result of the fabrication process, gets stiffened by the epoxy resin and acts like flat ribs when embedded in concrete. The mechanical interlock results in a very stiff bond behaviour and a high bond strength, which in turn leads to smaller crack distances and crack widths. However, this induces high bond stresses in the concrete which, in combination with a flat fibre

strand geometry, can lead to a longitudinal cracking in TRC [13, 14]. Once such a longitudinal cracking occurs the bond performance is decreased, which in turn negatively affects the crack width. Another important aspect that influences the bond of TRC is the surface finish, where an additional sand-coating has proven to significantly enhance the bond-performance [15]. All those various effects make the prediction of crack widths and crack distances in TRC rather complex, which is why further investigations are needed.

This manuscript presents a comprehensive experimental study on the cracking behaviour of epoxy impregnated TRC. For this purpose, uniaxial tensile tests were performed on TRC-specimens reinforced with different types of epoxy-impregnated fabrics. The types of reinforcement differ in their geometric properties as well as in their surface finish (smooth or sand coated). To account for a possible influence of the concrete cover, the element thickness was additionally varied. A total of 48 specimens was tested. By observing the behaviour using advanced measurement methods such as Digital Image Correlation (DIC), a sound understanding of the cracking behaviour of epoxy-impregnated textile reinforcement can be gained.

2. EXPERIMENTAL PROGRAMME

2.1. Test setup

To evaluate the cracking behaviour under uniaxial tension, a tensile test setup is developed following the recommendations given in literature [16]. TRC plates were clamped between anchorage plates of dimensions $120 \times 120 \text{ mm}^2$ with a force C of 50-70 kN. These plates are connected to the testing machine through hinges (Figure 1). This allows for a centric alignment of the specimen. The samples size was $800 \times 120 \text{ mm}$. Three adjacent fibre strands of the used textile reinforcement that had a mesh width of 38 mm (see Section 2.2.2) can be placed within the specimen. The length was chosen to exceed five times the length of the anchorage zone to minimize disturbances within the free length. For the tested configurations (see section 2.2.2) where reinforcement was placed in the weft direction, three specimens were cast, while for the warp direction, one specimen only was cast for comparison.

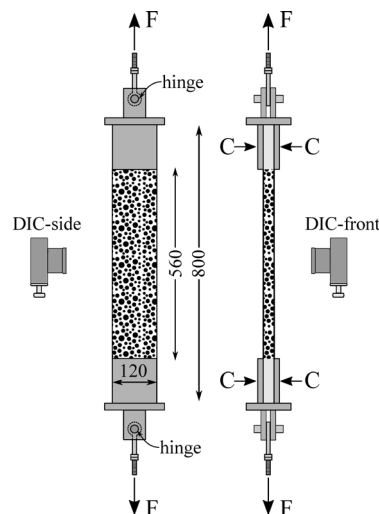


Figure 1: Test setup for the uniaxial tensile tests; note that the actual distance of the DIC measurement system to the specimen was bigger than indicated in this figure.

The tests were carried out under the displacement controlled at a velocity of 1 mm/m. The load was measured during testing with a load cell integrated into the testing machine. To obtain detailed information on the crack progression, including a continuous observation of crack distances and crack widths, DIC measurements were carried out on both the side and the front of the specimen.

2.2. Materials

2.2.1. Concrete

A fine-grained concrete was used in this study. The main components of the concrete mix design are shown in Table 1. Smaller portions of additives for shrinkage compensation, hardening acceleration and air entrainment were also added. For a detailed description of the concrete mix design, see [17].

Table 1: Main components of the concrete mix design of the mix used in this study

CEM I 42.5R [kg/m ³]	Microsilica [kg/m ³]	Limestone Powder [kg/m ³]	Sand 0/1 mm [kg/m ³]	Water [kg/m ³]	Superplasticizer [kg/m ³]
569.16	62.61	113.83	1419.08	164.1	22.77

A series of tests was carried out to characterize the concrete behaviour. This included compression tests on cubes of dimensions 100x100x100 mm³ as well as prismatic test specimens with dimensions 40x40x160 mm³ following EN 196-1 [18]. The tensile strength of the concrete f_{ctm} as well as the young's modulus in tension E_{cm} could therefore be determined. To perform the tests, the prismatic specimens were notched in the middle and glued to steel plates on both end faces. These steel plates were then connected to the testing machine by a hinge. The test specimens were loaded displacement controlled till a failure occurred in the notched area. The residual area was measured and used to calculate the tensile strength. The broken end surfaces were then polished and the steel plates were glued once more on both end faces in order to determine the young's modulus. For this purpose, three load cycles were performed with an upper and a lower bound of one third and one-tenth of the tensile strength, respectively. An additional set of prisms was used to test the flexural tensile strength $f_{ctm,n}$ by means of three-point bending tests. It is worth mentioning that the uniaxial tensile strengths of the concrete batches used for the specimens with sand-coated (Series S) and uncoated fabrics (Series U) differ substantially (See Table 2).

Table 2: Material properties of the concrete (mean value and standard deviation)

type	f_{cm} [N/mm ²]	f_{ctm} [N/mm ²]	$f_{ctm,n}$ [N/mm ²]	E_{cm} [N/mm ²]
S	124.62 (±8.95)	6.78 (±0.7)	13.66 (±1.31)	36961.49 (±1480.79)
U	124.01 (±2.71)	8.75 (±0.51)	14.76 (±1.03)	36978.46 (±910.82)

2.2.2. Textile reinforcement

In this study, a textile reinforcement from the company solidian was used. The reinforcement was listed in their portfolio as Grid Q142-CCE-38-E5. The epoxy-impregnated fibre strands have a net fibre cross-section area of 5.42 mm². To determine the breaking strength f_{tu} and strain ϵ_{tu} as well as the young's modulus E_t , individual fibre strands were clamped into a testing machine and tested under uniaxial tension. To avoid a premature failure due to high lateral stresses during clamping, a sleeve was placed over the end of the fibre strands and subsequently filled with expansive mortar [19]. After hardening of the mortar (≥ 24 hours), the actual testing was carried out and results summarized in Table 4. It is noticeable that the measured values surpass the values specified by the manufacturer in all cases. In the following sections, the reinforcement is named according to the surface finish (S – sand-coated or U – uncoated) followed by the direction of the fibre strand (WA - warp or WE – weft). It is worth mentioning that uncoated in this context does not mean that these fabrics aren't impregnated but rather that they don't have an additional sand-coating applied.

Table 3: Material properties of the textile reinforcement (mean value and standard deviation).

type	f_{tu} [N/mm ²]	ϵ_{tu} [N/mm ²]	E_t [GPa]
S-WA	3280 (±287)	1.38 (±0.09)	2379 (±275)
S-WE	3963 (± unspecified)	1.73 (± unspecified)	2291 (± unspecified)
U-WA	3789 (±173)	1.56 (±0.12)	2430 (±150)
U-WE	3939 (±260)	1.55 (±0.05)	2546 (±108)

3. DATA CURATION AND PROGRESSION

The front surface DIC observations give information on the crack-width w_{cr} progression by creating two adjacent curves besides the crack and evaluating the curve distance during loading. The obtained data was then synchronized with the time-dependent load measurements of the testing machine. This allows for a continuous evaluation of all the cracks and their respective crack-width during loading. Figure 2 shows the crack-width progression during loading for an uncoated (left) and a sand-coated fabric (right) in the weft direction. Distinct differences are observed: the uncoated fabric sample exhibits fewer cracks with much larger crack-widths.

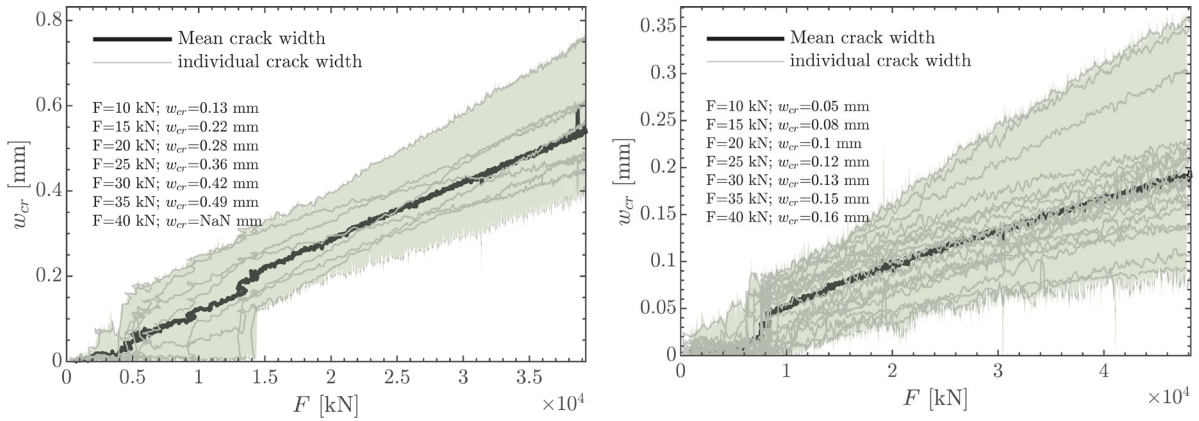


Figure 2: Continuous measurement of crack-width during loading for a specimen with an uncoated (left) and sand-coated (right) textile in case of a reinforcement ratio equal to 0.92%; note that the y-scale is different

Table 4 shows the crack width (mean value and standard deviation) at load stages 10:5:40 (initial load stage: step change: max load stage) for each configuration described in this manuscript. As the concrete cover increases, which corresponds to a lower reinforcement ratio ρ , the cracking load gets progressively larger, meaning that the specimen is still uncracked below this tensile force. Hence, no crack width can be evaluated. This is indicated in the table with NaN. On the other hand, if the specimen has not exceeded individual load stages due to a prior failure (e.g. U-WA; $\rho = 0.92$), the table entry is also listed as NaN.

Table 4: Crack width at different load stages for the TRC specimens with uncoated and sand-coated textile fabrics

	ρ	S_{cr}	$w_{cr,10}$	$w_{cr,15}$	$w_{cr,20}$	$w_{cr,25}$	$w_{cr,30}$	$w_{cr,35}$	$w_{cr,40}$
	[%]	[mm]	[mm]	[mm]	[mm]	[mm]	[mm]	[mm]	[mm]
S-WA	0.92	19.73 (± 8.42)	0.09 (± 0.03)	0.12 (± 0.04)	0.15 (± 0.04)	0.18 (± 0.06)	0.19 (± 0.07)	0.21 (± 0.08)	0.23 (± 0.08)
S-WA	0.55	18.92 (± 7.5)	0.1 (± 0)	0.11 (± 0.04)	0.13 (± 0.06)	0.14 (± 0.06)	0.16 (± 0.07)	0.17 (± 0.08)	0.18 (± 0.09)
S-WA	0.39	21.68 (± 7.27)	NaN	0.03 (± 0)	0.13 (± 0.06)	0.14 (± 0.07)	0.16 (± 0.08)	0.18 (± 0.08)	0.21 (± 0.1)
S-WA	0.30	43.58 (± 13.19)	NaN	NaN	0.30 (± 0.19)	0.34 (± 0.2)	0.38 (± 0.21)	0.44 (± 0.23)	0.45 (± 0.25)
S-WA	0.25	NaN	NaN	NaN	NaN	NaN	NaN	NaN	NaN
S-WA	0.21	42.05 (± 12.77)	NaN	NaN	NaN	NaN	0.37 (± 0.21)	0.47 (± 0.2)	0.52 (± 0.23)
S-WE	0.92	21.1 (± 7.84)	0.06 (± 0.02)	0.08 (± 0.03)	0.1 (± 0.04)	0.11 (± 0.04)	0.13 (± 0.05)	0.15 (± 0.06)	0.16 (± 0.06)
S-WE	0.55	19 (± 6.87)	NaN	0.11 (± 0.05)	0.14 (± 0.06)	0.16 (± 0.07)	0.19 (± 0.08)	0.21 (± 0.09)	0.24 (± 0.09)
S-WE	0.39	21.14 (± 9.9)	NaN	NaN	0.07 (± 0.07)	0.16 (± 0.08)	0.18 (± 0.09)	0.20 (± 0.09)	0.22 (± 0.1)
S-WE	0.30	33.56 (± 11.95)	NaN	NaN	NaN	0.2 (± 0.16)	0.36 (± 0.16)	0.41 (± 0.19)	0.45 (± 0.21)
S-WE	0.25	39.58 (± 16.07)	NaN	NaN	NaN	NaN	NaN	0.44 (± 0.17)	0.49 (± 0.18)
S-WE	0.21	48.56 (± 18.08)	NaN	NaN	NaN	NaN	NaN	NaN	0.46 (± 0.4)
U-WA	0.92	35.93 (± 10.48)	0.17 (± 0.05)	0.17 (± 0.06)	0.2 (± 0.06)	0.24 (± 0.06)	0.29 (± 0.07)	NaN	NaN
U-WA	0.55	54.26 (± 20.49)	NaN	0.04 (± 0.01)	0.3 (± 0.21)	0.45 (± 0.28)	0.53 (± 0.31)	0.58 (± 0.31)	0.65 (± 0.31)
U-WA	0.39	174.78 (± 77.67)	NaN	NaN	NaN	NaN	1.02 (± 0.07)	1.18 (± 0.12)	1.76 (± 0.46)

U-WA	0.30	71.12 (± 31.11)	NaN	NaN	NaN	0.38 (± 0.25)	0.56 (± 0.39)	0.76 (± 0.52)	0.88 (± 0.59)
U-WA	0.25	75.29 (± 16.4)	NaN	NaN	NaN	NaN	0.6 (± 0.05)	0.72 (± 0.08)	0.83 (± 0.12)
U-WA	0.21	78.12 (± 4.48)	NaN	NaN	NaN	0.54 (± 0.15)	0.66 (± 0.19)	0.73 (± 0.18)	0.81 (± 0.17)
U-WE	0.92	53.78 (± 26.83)	0.15 (± 0.07)	0.21 (± 0.08)	0.26 (± 0.1)	0.32 (± 0.12)	0.36 (± 0.14)	0.41 (± 0.16)	0.13 (± 0.21)
U-WE	0.55	115.79 (± 31.49)	NaN	0.48 (± 0.22)	0.48 (± 0.18)	0.64 (± 0.15)	0.78 (± 0.19)	0.99 (± 0.31)	1.13 (± 0.39)
U-WE	0.39	142.27 (± 56.13)	NaN	NaN	NaN	0.41 (± 0.5)	0.65 (± 0.48)	1.12 (± 0.33)	1.29 (± 0.34)
U-WE	0.30	157.48 (± 97.58)	NaN	NaN	NaN	NaN	NaN	1.76 (± 1.31)	1.08 (± 0.68)
U-WE	0.25	149.45 (± 0)	NaN	NaN	NaN	NaN	NaN	NaN	5.84 (± 1.76)
U-WE	0.21	267.5 (± 29.5)	NaN	NaN	NaN	NaN	NaN	2.75 (± 0.72)	NaN

4. RESULTS

Table 4 gives a very condensed overview of the crack development during loading of TRC elements reinforced with different types of textile reinforcement. To evaluate the difference between the individual configurations, the crack width progression is visually compared in Figure 3 for a reinforcement ratio $\rho = 0.55\%$ (corresponds to a concrete cover at each side of 10 mm), with the applied force given on the x-axis while the y-axis indicated the corresponding crack width. When comparing the uncoated fabrics in the weft and warp direction, it can be seen that the crack-width is potentially larger in the weft direction compared to the warp direction. Possible explanations for this observation are given in Section 5.1. Note that no crack-width was measured in warp direction below 25 kN. This is because first cracks only occurred just after exceeding 20 kN due to the scatter of the tensile strength of the concrete. When comparing the sand-coated fabrics, it is noticeable that the corresponding crack widths are significantly smaller than for the uncoated fabrics (see Figure 4 left and right). When comparing the weft and warp direction of the sand-coated fabrics also a slight trend of higher crack-widths can be noticed for the warp direction, but this does not appear to be a significant difference, since the envelope curves of the standard deviation for both types widely overlap.

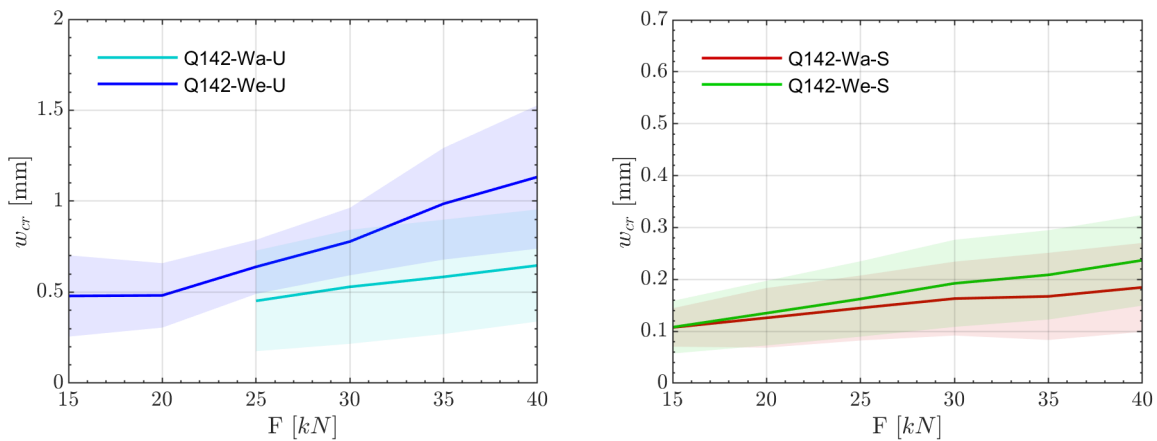


Figure 3: Comparison of the crack-width progression during loading for the uncoated (left) as well as sand-coated fabrics (right) in weft and warp direction for both cases

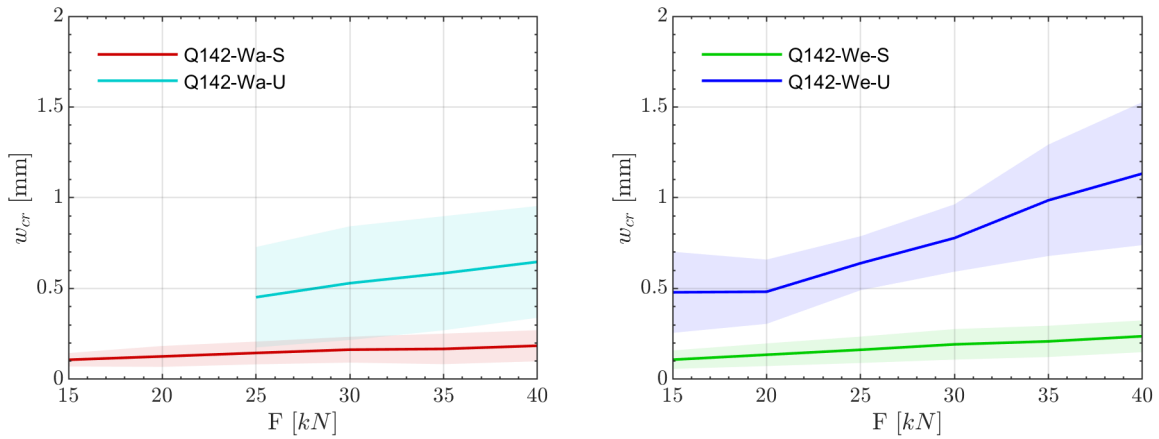


Figure 4: Comparison of the crack-width progression during loading for the warp (left) as well as the weft thread (right) between the uncoated and the sand-coated fabric

Important aspects regarding the influence of the concrete cover on the cracking behaviour become clearer when comparing the crack progression (y-axis) during loading for the individual reinforcement ratios ρ (displayed on the x-axis). In Figure 5 left, where the crack progression is shown for the uncoated fabrics in the weft and warp direction, it can again be seen that the crack widths are considerably higher in the weft direction, indicating a stronger bond performance in the warp direction. This trend can be observed over the entire range of tested reinforcement ratios. It can also be seen, that the crack widths are nearly constant at the individual load stages for a range of the reinforcement ratio between 0.21-0.55 % and then decreases for even larger reinforcement ratios. The significantly higher crack widths for the weft thread at reinforcement ratios of 0.3 and 0.39 % are due to an occurring anchorage failure here, which led to an excessive opening of one crack. A contrasting behaviour is observed for the sand-coated fabrics. While for higher reinforcement ratios the crack-width is relatively constant within a range of 0.39-0.92 %, a significantly higher crack width is observed at reinforcement ratios below 0.39 %. This goes in line with a splitting crack that occurred while loading. Comparing the crack width progression of the uncoated and sand-coated fabrics in each individual direction, the different behaviours previously described become apparent with a generally smaller crack width in the case of the sand-coated fabrics (see Figure 6).

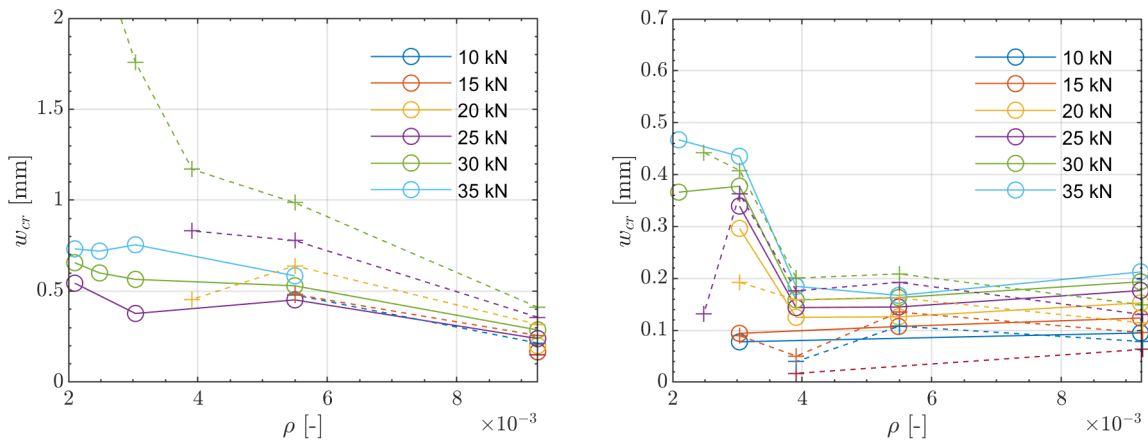


Figure 5: Comparison of the crack-width progression during loading for the uncoated (left) as well as sand-coated fabrics (right) in weft and warp direction for both cases

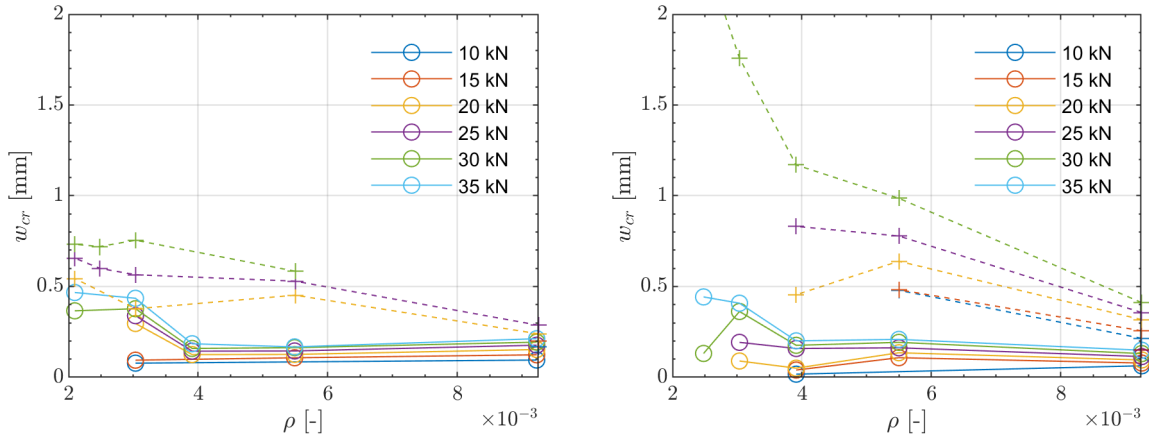


Figure 6: Comparison of the crack-width progression during loading for the warp (left) as well as the weft thread (right) between the uncoated and the sand-coated fabric

5. DISCUSSION

5.1. Difference in crack-width between weft and warp thread

In light of the results presented in Section 4, some significant differences can be noticed. While it is obvious that the smaller crack widths in the case of the sand-coated fabrics result from a significantly improved bond performance due to the rough structure created by the additional coating on the surface of the fabric, the reason behind the distinct difference in the crack-width between the weft and warp direction of the uncoated fabrics remained unclear. Laser scans were therefore conducted to capture the overall geometry of the fibre strands (see Figure 7). As no remarkable difference in the repeating variation in cross-sectional dimension and the cross-sectional geometry is noticeable, it is assumed that the difference is mainly coming from the knitting thread that wraps the warp thread. Whether the knitting thread increases friction or locally compresses the yarn so that an interlocking effect is enabled, is beyond the scope of this work.

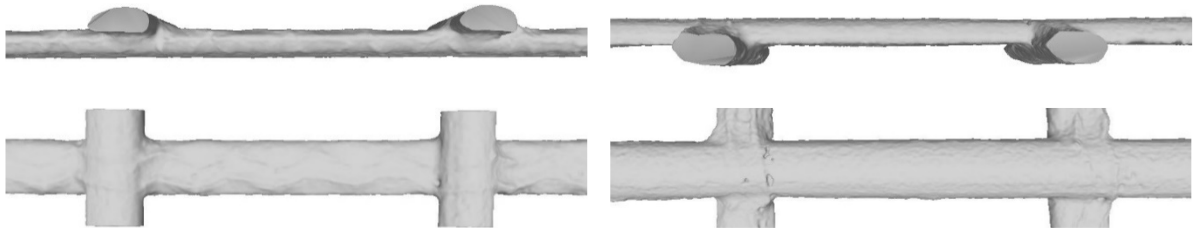


Figure 7: Ground view (top) and side view (bottom) of warp (left) and weft (right) fibre strand

5.2. Influence of the reinforcement ratio on the crack width

A decisive influence of the reinforcement ratio on the crack width is shown in section 4. In both the uncoated and the sand coated fabrics, there is a transition point in the reinforcement ratio at which the crack width progression changes. This transition occurs at $\rho = 0.55\%$ for the uncoated fabrics, with the overall crack width transitioning from being roughly constant to decreasing. The sand-coated fabrics show a transition at around 0.39% but with an opposite behaviour: the crack width increases significantly with reinforcement ratio below the transition value and then becomes constant above. In both cases – uncoated and sand coated fabric – splitting cracks in the layer of the reinforcement occur when the reinforcement ratio is smaller or equal to the reinforcement ratio at the transition point. In the

case of the sand-coated fabrics, it seems evident that the formation of the splitting cracks leads to a decrease in the bond performance. It was however not clear, at first glance, why the formation of splitting cracks in the uncoated fabrics does not cause a significant increase in crack widths. An evaluation of the DIC measurements sheds some light on this matter. The splitting cracks start from an initial transverse crack and cause secondary transverse cracks which propagate from the crack tip of the splitting crack. This leads to a somewhat paradoxical situation, in which the crack width does not increase significantly although the bond performance is decreased, as more transverse cracks are present. It should be noted that this is an initial assumption based on preliminary observations. Further investigations are necessary to substantiate this theory.

6. CONCLUSIONS

The cracking behaviour of TRC is an important topic that affects the serviceability limit of structures. The reinforcement has a high resistance to corrosion, but limitations linked to crack widths may arise from other aspects such as aesthetics, chemical ingress etc. While the bearing capacity of TRC has been widely studied in recent years, the cracking behaviour still lacks a coherent investigation. In this manuscript, a total of 48 test specimens were evaluated with respect to the cracking behaviour under uniaxial tension. Besides testing both the weft and warp thread, the reinforcement ratio was varied and fabrics with an additional sand-coating were part of this study. The following conclusions can be drawn from this study:

- The crack-width progressions for the weft and warp thread of uncoated fabrics differ significantly, with the specimens reinforced with fabrics in warp direction exhibiting smaller crack widths. While the overall geometric properties are roughly similar the difference is attributed to the additional knitting thread that wraps the warp thread.
- The application of an additional-sand coating has a decisive influence on the cracking behaviour of TRC. The sand coating creates a rough surface on the fabrics, enabling a mechanical interlocking with the surrounding cementitious matrix. This is accompanied by significantly lower crack widths.
- The reinforcement ratio has a decisive influence on the cracking behaviour of TRC. In the case of uncoated fabrics, a progressive splitting cracking behaviour that initiates secondary transverse cracks was observed at lower reinforcement ratios. This leads to smaller than expected crack widths at small reinforcement ratios, although the bond performance is decreased due to the splitting cracks. For sand-coated fabrics, an opposite trend is observed, where a lower reinforcement ratio leads to increased crack-widths. We attribute this effect to a decreased bond performance caused by the splitting cracks.

The results presented in this manuscript are an excerpt from a much larger study. The hypothesis arising from the evaluation of the specific fabric that is described in this study will be verified by evaluating the cracking behaviour of other fabrics. It has also been shown that the cracking behaviour is very much influenced by the concrete cover and the occurrence of any splitting cracks. A detailed evaluation of this cracking mode will follow.

ACKNOWLEDGEMENT

This project has received funding from the European Union's Horizon 2020 research and innovation programme under the Marie Skłodowska-Curie grant agreement No 101027058

DATA AVAILABILITY

The data supporting the findings of this study are available on request from the corresponding authors.

REFERENCES

- [1] Reichenbach, S.; Preinstorfer, P.; Hammerl, M.; Kromoser, B. A review on embedded fibre-reinforced polymer reinforcement in structural concrete in Europe, *Construction and Building Materials*. **2021**, *307*, 124946. <https://doi.org/10.1016/j.conbuildmat.2021.124946>
- [2] Kromoser, B.; Preinstorfer, P.; Kollegger, J. Building lightweight structures with carbon-fiber-reinforced polymer-reinforced ultra-high-performance concrete: Research approach, construction materials, and conceptual design of three building components, *Structural Concrete*. **2019**, *20*, 730-744. <https://doi.org/10.1002/suco.201700225>
- [3] Scholzen, A.; Chudoba, R.; Hegger, J. Thin-walled shell structures made of textile-reinforced concrete, *Structural Concrete*. **2015**, *16*, 106-114. <https://doi.org/10.1002/suco.201300071>
- [4] Sharei, E.; Scholzen, A.; Hegger, J.; Chudoba, R. Structural behavior of a lightweight, textile-reinforced concrete barrel vault shell, *Composite Structures*. **2017**, *171*, 505-514. <https://doi.org/10.1016/j.compstruct.2017.03.069>
- [5] Helbig, T.; Unterer, K.; Kulas, C.; Rempel, S.; Hegger, J. Pedestrian bridge made from carbon-concrete in Albstadt-Ebingen – First entirely carbon-reinforced concrete bridge worldwide, *Beton- und Stahlbetonbau*. **2016**, *111*, 676-685. <https://doi.org/10.1002/best.201600058>
- [6] Dvorkin, D.; Poursaee, A.; Peled, A.; Weiss, W. J. Influence of bundle coating on the tensile behavior, bonding, cracking and fluid transport of fabric cement-based composites, *Cement and Concrete Composites*. **2013**, *42*, 9-19. <https://doi.org/10.1016/j.cemconcomp.2013.05.005>
- [7] Curbach, M.; Jesse, F. Specifications and Application of Textile Reinforced Concrete (TRC), *Beton- und Stahlbetonbau*. **2009**, *104*, 9-16. <https://doi.org/10.1002/best.200800653>
- [8] El Ghadioui, R.; Proske, T.; Tran, N. L.; Graubner, C.-A. Structural behaviour of CFRP reinforced concrete members under bending and shear loads, *Materials and Structures*. **2020**, *53*, 63. <https://doi.org/10.1617/s11527-020-01496-7>
- [9] Bielak, J.; Schmidt, M.; Hegger, J.; Jesse, F. Structural Behavior of Large-Scale I-Beams with Combined Textile and CFRP Reinforcement, *Applied Sciences*. **2020**, *10*, 1-26. <https://doi.org/10.3390/app10134625>
- [10] Preinstorfer, P.; Kromoser, B.; Kollegger, J. Categorisation of the bond behaviour of textile reinforced concrete, *Bauingenieur*. **2019**, *94*, 416-424.
- [11] Preinstorfer, P.; Kollegger, J. New insights into the splitting failure of textile-reinforced concrete, *Composite Structures*. **2020**, *243*, 1-10. <https://doi.org/10.1016/j.compstruct.2020.112203>
- [12] Bielak, J.; Spelter, A.; Will, N.; Claßen, M. Anchorage behavior of textile reinforcement in thin concrete components, *Beton- und Stahlbetonbau*. **2018**, *113*, 515-524. <https://doi.org/10.1002/best.201800013>
- [13] Preinstorfer, P.; Kromoser, B. Influence of geometrical parameters on the splitting forces in textile-reinforced concrete, *Materials and Structures*. **2020**, *53*, 1-17. <https://doi.org/10.1617/s11527-020-01590-w>
- [14] Beßling, M.; Orłowsky, J. Quantification of the Influence of Concrete Width per Fiber Strand on the Splitting Crack Failure of Textile Reinforced Concrete (TRC), *Polymers*. **2022**, *14*, 489. <https://doi.org/10.3390/polym14030489>
- [15] Bielak, J.; Rempel, S.; Felber, M.; Durst, H.-J.; Will, N. Rehabilitation of the bridge Rheinsteg near Albruck with carbon reinforced concrete, *Beton- und Stahlbetonbau*. **2021**, *116*, 488-497. <https://doi.org/10.1002/best.202100024>
- [16] Schütze, E.; Bielak, J.; Scheerer, S.; Hegger, J.; Curbach, M. Uniaxial tensile test for carbon reinforced concrete with textile reinforcement, *Beton- und Stahlbetonbau*. **2018**, *113*, 33-47. <https://doi.org/10.1002/best.201700074>
- [17] Yanik, S. *Effect of the concrete cover to cracking of HPC with carbon reinforcement under uniaxial tensile load*. TU Wien, 2021. Master thesis.
- [18] *ÖNORM EN 196-1*. Austrian Standards Institute (ON), Vienna, 2005.
- [19] Lees, J. M.; Gruffydd-Jones, B.; Burgoyne, C. Expansive cement couplers: A means of pre-tensioning fibre-reinforced plastic tendons, *Construction and Building Materials*. **1995**, *9*, 413-423. [https://doi.org/10.1016/0950-0618\(95\)00070-4](https://doi.org/10.1016/0950-0618(95)00070-4)